Letter

Optical Excitation and Probing of Antiferromagnetic Modes with Nonuniform-in-depth Distribution in Birefringent Antiferromagnetic Crystals

A.A. Voronov,[1,2,*] D.O. Ignatyeva,[1,2,3] A.K. Zvezdin,[1,4] T.B. Shapaeva,[5] and V.I. Belotelov[1,2,3]

[1] *Russian Quantum Center, Moscow 121205, Russia*

[2] *Photonic and Quantum Technologies School, Lomonosov Moscow State University, Moscow 119991, Russia*

[3] *Institute of Physics and Technology, V.I. Vernadsky Crimean Federal University, Simferopol 295007, Crimea*

[4] *Prokhorov General Physics Institute, Russian Academy of Sciences, Moscow 119991, Russia*

[5] *Faculty of Physics, Lomonosov Moscow State University, Moscow 119991, Russia*

(Received 13 August 2021; accepted 5 October 2021; published 9 November 2021)

Optical pump-probe setups are commonly used for the excitation and investigation of spin dynamics in various types of magnetic materials. However, spatially homogeneous excitation is usually considered. In the present study, we describe an approach to optical excitation of nonuniform THz spin dynamics and to probing its spatial distribution inside a magnetic crystal. We propose to illuminate a crystal with laser pulses of properly adjusted polarization to benefit from the strong optical birefringence inherent in the crystal. This results in unusual behavior of the effective magnetic field generated by the pulses due to the inverse Faraday effect and the peculiar sign-changing dependence of the direct Faraday effect inside the crystal. The study is performed for an yttrium orthoferrite crystal as an example, although the proposed approach is applicable to various magnetic materials with optical anisotropy.

DOI: 10.1103/PhysRevApplied.16.L051001

Studies of spin-system dynamics are concerned with several different rapidly growing fields of technology, such as modern telecommunication technologies [1,2], quantum computing [3,4], several different approaches to magnetic data recording and reading [5–7], light modulation at GHz frequencies [8–11], biosensing [12], and magnetometry [13]. Antiferromagnetic materials, such as $YFeO_3$ and $DyFeO_3$, are promising candidates for practical use in high-speed devices, since they possess a large magneto-optical response [14–16] and allow the excitation of quasiantiferromagnetic modes at nearly THz frequencies [17–28]. Although these modes can be excited by THz electromagnetic pulses [23–25], optical excitation via femtosecond laser pulses is also very promising, since it has a local (at micrometer and even submicrometer scales) and tunable impact via various optomagnetic effects, including the inverse Faraday effect (IFE) [26–33], predicted by Pitaevskii [34] and further elaborated on and demonstrated a little later by Van der Ziel *et al.* [35] and Pershan *et al.* [36].

The IFE is related to impulsive stimulated Raman scattering [37,38] and does not require absorption of light, thus providing two main advantages: the optical impact is instantaneous and nonthermal [26]. In an isotropic magnetic medium, the effective magnetic field induced via the IFE is maximum for circularly polarized incident radiation and absent for linearly polarized radiation. The IFE-induced magnetic field is parallel to the wave vector of the light. However, in optically anisotropic materials, the situation is more complicated. Because of the conversion of the polarization of the light from an initial circular polarization to elliptical and then linear while propagating through the medium, the distribution of the IFE field becomes spatially nonuniform. Moreover, generally, the orientation of this field may not be parallel to the wave vector of the light [39]. Usually, this phenomenon is reported to complicate the analysis of spin dynamics [17], and several studies have been carried out to find out how to interpret the observed probe signal with respect to the polarization of the pump [17] or probe [40] pulse or both of them [31]. We focus our study on the IFE phenomenon; however, under certain conditions spin dynamics in antiferromagnets can be also excited via the inverse Cotton-Mouton effect [17]. In this case, pump-probe studies can be performed in a very similar way to that proposed in the present paper, and the results will be qualitatively the same.

Here we show that, in contrast to the well-known situation in isotropic materials, optical anisotropy provides a unique tool for the excitation and detection of spatially nonuniform spin dynamics. Such possibilities cannot be achieved in isotropic materials, due to the homogeneity of the IFE field inside the pumping area.

*andrey.a.voronov@gmail.com

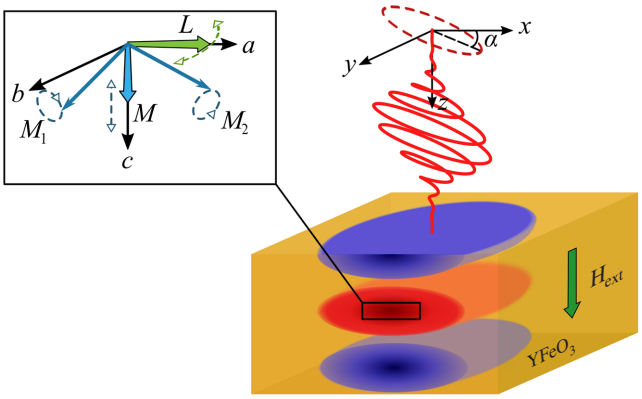

FIG. 1. Schematic representation of the configuration under study and the dynamics of the antiferromagnetism and magnetization vectors in the quasiantiferromagnetic mode (inset).

The IFE can be described in terms of the effective magnetic field $\mathbf{H}_{\mathrm{IFE}}$ induced by light,

$$\mathbf{H}_{\mathrm{IFE}} = -\frac{ig}{16\pi M_s}[\mathbf{E} \times \mathbf{E}^*], \tag{1}$$

where g is the magneto-optical gyration coefficient, M_s is the saturation magnetization, $\mathbf{E}$ is the electric field of the incident light, and $\mathbf{E}^*$ is its complex conjugate. Therefore, if the polarization of the electromagnetic field varies inside the magnetic material, $\mathbf{H}_{\mathrm{IFE}}$ also becomes inhomogeneous.

Consider a biaxial crystal in which the incident light propagates along a magnetic field that coincides with one of the optical axes of the crystal. Such a configuration may be implemented in various types of canted antiferromagnetic materials, including orthoferrites, that possess a high optical anisotropy and magneto-optical response. For definiteness, we consider the material yttrium orthoferrite ($YFeO_3$), with the c axis perpendicular to the sample plane (Fig. 1).$YFeO_3$ belongs to the family of rare-earth orthoferrites with an orthorhombic crystal structure. Below the Néel temperature, $YFeO_3$ behaves like a weak ferromagnet, with two Fe^{3+} sublattices coupled antiferromagnetically by an exchange interaction and aligned along the a crystal axis. The presence of the Dzyaloshinskii-Moriya interaction leads to a slight canting of the neighboring Fe^{3+} spins by an angle of 0.5° in such a way as to give the material a small macroscopic magnetization along the c crystal axis. In such a configuration, the diagonal elements of the permittivity tensor are $\varepsilon_{xx} = 2.365$, $\varepsilon_{yy} = 2.4$, $\varepsilon_{zz} = 2.337$, $\varepsilon_{xy} = -ig$, and $\varepsilon_{yx} = ig$, where $g = 0.001$ (other elements are equal to zero), so that $|\varepsilon_{ii} - \varepsilon_{jj}| \gg \varepsilon_{ij}$.

The polarization conversion in the material can be described using Jones matrices [14,41]. This allows one to calculate the distribution of the electric field along the coordinate of light propagation, knowing the initial polarization state $\mathbf{E}_z = \hat{J}\mathbf{E}_{z=0}$. The form of $\hat{J}$ for the configuration under study is presented in the Supplemental Material [42]. Let us take the initial polarization of the incident light to be in the form $(E_x, E_y)_{z=0} = [\cos\alpha, (\sin\alpha)e^{i\psi}]$, where α describes the angle between the polarization of the incident light and the a crystal axis, and ψ is the ellipticity angle that specifies the retardation between the two orthogonal polarizations. For example, $\alpha = 45°$ and $\psi = 0$ correspond to a linear initial polarization at an angle of 45° to the a crystal axis, and $\alpha = 45°$ and $\psi = \pm 90°$ correspond to circularly polarized incident light.

Since the medium investigated simultaneously possesses optically anisotropic and gyrotropic properties, the resulting distribution of the optical electric field, as well as that of the IFE field, depends strongly on the polarization and wavelength of the incident light (Fig. 2). Using Eq. (1) and the Jones matrix for the case considered (see the Supplemental Material [42]), one can obtain

$$H_{\mathrm{IFE}} = H^0_{\mathrm{IFE}} \sin(2\alpha_{\mathrm{pm}}) \sin\left(k_{\mathrm{pm}}\,\Delta n z + \psi_{\mathrm{pm}}\right), \tag{2}$$

where $\Delta n = \sqrt{\varepsilon_{xx}} - \sqrt{\varepsilon_{yy}}$ in the approximation $|g| \ll |\varepsilon_{xx} - \varepsilon_{yy}|$, which is valid for anisotropic antiferromagnets over a wide spectral range [41]; $H^0_{\mathrm{IFE}} = -g|\mathbf{E}|^2/(16\pi M_s)$ is the IFE magnitude for circularly polarized light; and k_{pm}, ψ_{pm}, and α_{pm} are the wave vector of the pump in vacuum and its ellipticity and polarization angles, respectively. Therefore, in this case the light induces H_{IFE}, which oscillates through the crystal-plate thickness in accordance with a harmonic law. The initial phase of the spatial distribution equals the ellipticity angle of the incident light ψ_{pm}. Consequently, by varying the ellipticity of the incident light, one can modify the initial phase of the spatial oscillations of the induced magnetic field along the direction of the crystal thickness [Figs. 2(a) and 2(c)–2(f)]. The second possibility is to tune the spatial frequency of such oscillations by changing the wavelength of the incident light [Fig. 2(b)]. At the same time, the amplitude of H_{IFE} is determined by the polarization angle of the incident light.

Let us now analyze how the inhomogeneous pattern of H_{IFE} launches spin dynamics in the antiferromagnetic crystal. Spin dynamics in an antiferromagnet can be described in terms of a unitary antiferromagnetism vector $\mathbf{L} = (\mathbf{M}_1 - \mathbf{M}_2)/(2M_0)$, where $\mathbf{M}_1$ and $\mathbf{M}_2$ are the magnetic moments of the sublattices, and M_0 is the saturation magnetization of each sublattice. In a spherical coordinate system with the polar axis aligned along the c crystal axis and the azimuthal axis along the a crystal axis, $\mathbf{L}$ has the following components: $\mathbf{L} = (\sin\theta\cos\varphi, \sin\theta\sin\varphi, \cos\theta)$.

The dynamics of $\mathbf{L}$ can be described in terms of the following linearized Euler-Lagrange equations, which are derived using the corresponding Lagrangian $\mathcal{L}$ and Rayleigh dissipation functions $\mathcal{R}$ [21,43–46] (for more

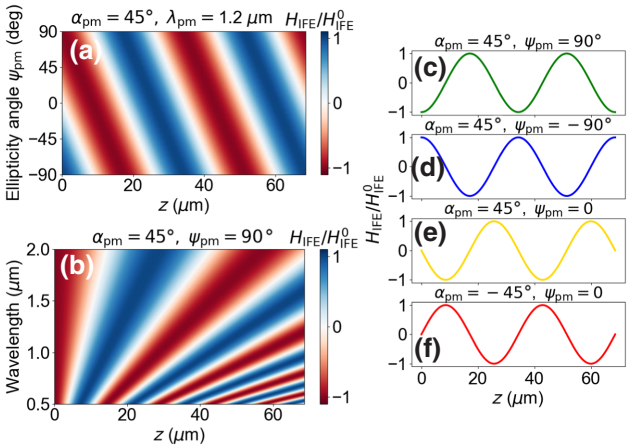

FIG. 2. IFE-induced effective magnetic field distribution inside *c*-cut yttrium orthoferrite (normalized to $H^0_{\rm IFE}$) vs (a) the ellipticity and (b) the wavelength of the incident light. (c)–(g) Effective magnetic field distributions generated by illumination with (c) right circularly polarized light ($\alpha = 45°$, $\psi = 90°$); (d) left circularly polarized light ($\alpha = 45°$, $\psi = -90°$); (e) light linearly polarized at an angle of $\alpha = 45°$ to the *a* crystal axis ($\psi = 0$); (f) light linearly polarized at an angle of $\alpha = -45°$ to the *a* crystal axis ($\psi = 0$).

details, see the Supplemental Material [42]):

$$\begin{cases} \ddot{\theta}_1 + \dfrac{2}{\tau}\dot{\theta}_1 + \omega_2^2\theta_1 = 0, \\ \ddot{\varphi}_1 + \dfrac{2}{\tau}\dot{\varphi}_1 + \omega_1^2\varphi_1 = \gamma\dot{H}_{\rm dr}, \end{cases} \tag{3}$$

where θ_1 and φ_1 are the small deviations of the angular variables θ and φ, $2/\tau = \zeta M_0\gamma/\chi_\perp$, $\omega_1 = \gamma\left[H_d\left(H_d - H_{\rm ext}\right) + 2K_b/\chi_\perp\right]^{(1/2)}$ and $\omega_2 = \gamma\left[H_d\left(H_{\rm ext} - 2H_d\right) + H^2_{\rm ext} - 2K_{\rm AC}/\chi_\perp\right]^{(1/2)}$ are the frequencies of the quasiantiferromagnetic and ferromagnetic modes, respectively, $H_{\rm ext} = 3$ kOe is the external magnetic field, $H_d = 150$ kOe is the effective magnetic field of the Dzyaloshinskii-Moriya interaction, $K_{\rm AC}$ and K_b are the magnetic anisotropy constants, $\chi_\perp$ is the transverse susceptibility of the material, $\gamma = 1.73 \times 10^7$ is the gyromagnetic ratio, ζ is the dimensionless Gilbert damping constant, and $H_{\rm dr}$ is the external driving force that appears due to the IFE. For a Gaussian optical pulse, $H_{\rm dr} = H_{\rm IFE}(z)\exp\left[-t^2/(2\,\Delta t^2)\right]$, where Δt is the pulse duration and $H_{\rm IFE}(z)$ is given by Eq. (2). Notice that spatial derivatives of θ_1 and φ_1 are neglected in Eq. (3) due to the slow variation in space, so that the coordinate z appears in Eq. (3) only as a parameter describing the driving field $H_{\rm dr}$.

Let us focus on the quasiantiferromagnetic mode. The calculated frequency ω_1 is about 0.52 THz, which is in good agreement with recently reported experimental values [19,23]. The first equation in the system of Eq. (3) gives $\theta_1 = 0$, and the solution of the second equation is $\varphi_1 \sim \sin(\omega_1 t + \beta)$, where β is the phase shift. The exact form of the solution is presented in the Supplemental Material [42]. Thus, the antiferromagnetism vector $\mathbf{L}$ oscillates in the *a*-*b* crystallographic plane (see the inset of Fig. 1). The dynamic component of the magnetization is given by the expression $\mathbf{M_d} = \chi_\perp[\mathbf{L} \times \dot{\mathbf{L}}]/\gamma$. Using the solutions obtained, one can derive the components of the dynamic magnetization $\mathbf{M_d} = (0, 0, M_d)$, where M_d is given by

$$M_d = H_A\chi_\perp \exp\left(-\frac{t}{\tau}\right)\sin\left(\omega_1 t + \xi\right), \tag{4}$$

where

$$H_A = \frac{H_{\rm IFE}(z)\omega_1\varkappa^2\sqrt{2\pi}}{\Delta\omega}\exp\left(-\frac{\omega_1^2 - 1/\tau^2}{2\,\Delta\omega^2}\right), \tag{5}$$

$\Delta\omega = 10^{13}$ rad/s is the spectral width of the laser pulse, which corresponds to the pulse duration $\Delta t = 100$ fs, $\varkappa = \sqrt{1 + 1/(\omega_1\tau)^2}$, and $\xi = \beta - \arcsin\varkappa^{-1}$. Thus the amplitude and the initial phase of such a quasiantiferromagnetic mode have a strong spatial dependence, so that such modes are labeled as inhomogeneous quasiantiferromagnetic (IQ-AFM) modes hereafter. The full adjustability of the spatial distribution of the driving force $H_{\rm IFE}$ [Figs. 2(a) and 2(b)] allows one to excite IQ-AFM modes with a harmonic distribution along the *c* axis.

There is still much uncertainty about how optical birefringence of the probe together with a complex spatial profile of the mode act on the observed probe signal, although some studies describing certain special cases numerically have been carried out [31]. Optical birefringence is usually treated as an unfavorable effect in the pump-probe technique and in some cases can be reduced by tuning the crystal composition [47]. Here we aim to develop a general analytical theory of the pump-probe technique in the presence of birefringence. This is especially important for spin modes characterized by a vanishing integral $\int_0^h M_d(z)\,dz = 0$ (where h is the crystal thickness), which cannot be detected in isotropic materials, since the full Faraday rotation of the probe polarization is zero in this case.

We consider the probe polarization to be aligned along the *a* crystal axis. For a homogeneous magnetization of an optically anisotropic crystal, the Faraday rotation has an oscillatory behavior along the optical axis due to the birefringence [41], $\Phi = -g\sin(k_{\rm pb}\Delta n z)/\Delta\varepsilon$, where $k_{\rm pb} = 2\pi/\lambda_{\rm pb}$. When the amplitude of the precession of the magnetization with time, $M_d^A(z)$, oscillates along the z axis, the gyration acquires an oscillating term as well, $g(z) = g_0 M_d^A(z)/M_s$, and the resulting Faraday rotation of the probe caused by the oscillating magnetization can be calculated from

$$\Phi_{\rm osc} = -\int_0^h \frac{g_0}{\Delta\varepsilon}\frac{M_d^A(z)}{M_s}k_{\rm pb}\,\Delta n\cos\left(k_{\rm pb}\Delta n z\right)dz. \tag{6}$$

It should be noted that while the oscillating part of the magnetization is induced via the IFE in the present case, the considerations below are valid for any mechanism of a harmonic magnetization distribution.

According to Eqs. (2) and (4), $M_d^A(z) \sim \sin(k_{\rm pm}\Delta n z + \psi_{\rm pm})$, and the probe Faraday rotation is determined by the correlation between the phases and frequencies of the harmonic functions in the integral in Eq. (6). Actually, Eq. (6) gives a clear picture of how the probe wavelength can be tuned to allow one to see the desired IQ-AFM mode and explains why it is possible to probe spin modes with $\int_0^h M_d^A(z)\,dz = 0$, which is impossible in an isotropic medium regardless of the probe wavelength. Figure 3(a) shows that for every value of the pump ellipticity, it is possible to tune the wavelength of the probe pulse in order to detect the spin oscillations caused by the nonuniform IQ-AFM mode. The value $M_d^A/M_s \sim 0.01$ is chosen in the present considerations as a typical value of the magnetization precession amplitude for $YFeO_3$. Notice that, in the case of a single-color pump-probe experiment ($\lambda_{\rm pm} = \lambda_{\rm pb} = 1.2\ \mu$m) [black dashed line in Fig. 3(a)], if the initial pump polarization is linear ($\psi_{\rm pm} = 0$), the amplitude of the Faraday-effect oscillations is zero due to the presence of two harmonic functions of different symmetry in the integral in Eq. (6). The maximum values of the probe Faraday-effect oscillations take place near the condition of coincidence of the spatial distribution of the effective magnetic field $H_{\rm IFE}$ with the derivative of the polarization conversion of the probe pulse [$\cos(k_{\rm pb}\Delta n z)$]; however, the optimal wavelength is slightly blueshifted [see Fig. 3(a)] due to the multiplication by $k_{\rm pb}$ in the integral in Eq. (6).

An expression for the oscillating part of the magnetically induced probe ellipticity $\Psi_{\rm osc}$ can be derived similarly to Eq. (6).

The distribution of the magnetization induced via IFE can be found after combining the expressions for the Faraday rotation $\Phi_{\rm osc}$ and ellipticity $\Psi_{\rm osc}$ of the probe pulse (for more details, see the Supplemental Material [42]):

$$M_d^A(z) = -\frac{M_s}{2\pi}\int_{-\infty}^{+\infty} \frac{\Delta\varepsilon\,(\Phi_{\rm osc} + i\Psi_{\rm osc})}{g_0 k_{\rm pb}\,\Delta n} \exp\left(-ik_{\rm pb}\,\Delta n z\right) d(k_{\rm pb}\,\Delta n). \quad (7)$$

Note that although in the present study the wavelength dependences of $\Delta\varepsilon$ and g are neglected, all basic results described by Eqs. (2), (6), and (7) remain valid under the substitution of $\Delta\varepsilon(\lambda)$ and $g(\lambda)$ for the corresponding material.

The expression obtained is particularly useful for studying an inhomogeneous magnetization. It allows one to reconstruct the distribution of the inhomogeneous magnetization, including that induced by an incident pump pulse via the IFE, $H_{\rm IFE}(z)$, using the measured spectral dependences of the Faraday effect $\Phi_{\rm osc}$ and ellipticity $\Psi_{\rm osc}$ of the probe pulse. Figure 4 shows the whole process. Notice that even if such measurements are performed in a limited spectral range [Figs. 4(a) and 4(b)], the magnetization distribution reconstructed through Eq. (7) [Fig. 4(d)] is in solid agreement with the real field [Fig. 4(c)].

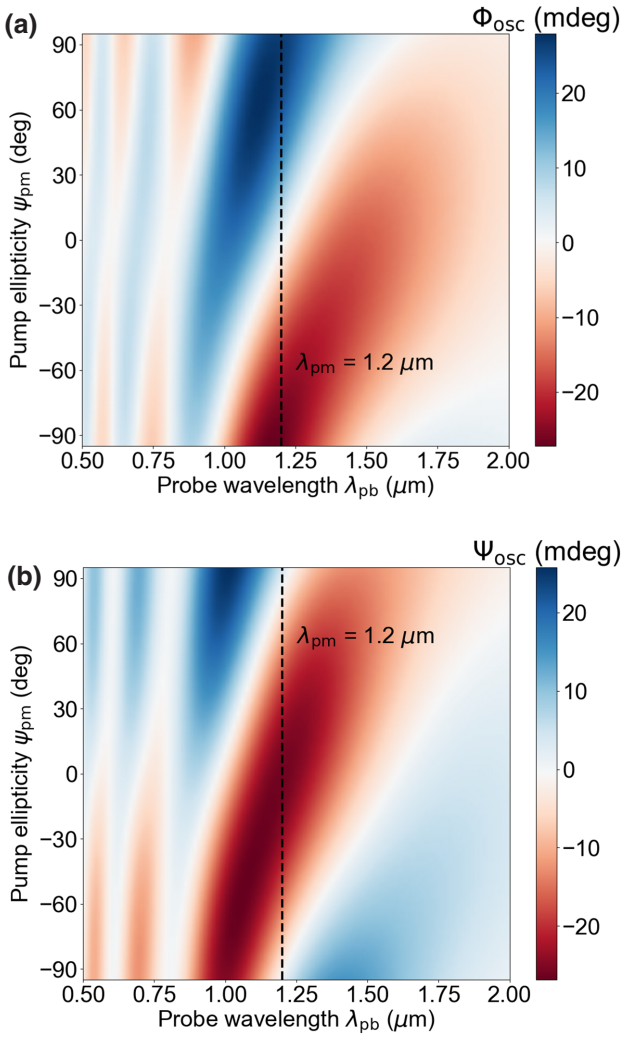

FIG. 3. Amplitude (taking account of sign) of the temporal oscillations in the probe polarization $\Phi_{\rm osc}$ (a) and induced ellipticity $\Psi_{\rm osc}$ (b) depending on the wavelength $\lambda_{\rm pb}$ of the probe and the ellipticity angle $\psi_{\rm pm}$ of the pump pulses. The wavelength of the pump pulse ($\lambda_{\rm pm} = 1.2\ \mu$m) and the length of the crystal ($h = 68.6\ \mu$m) are chosen in such a way to provide excitation of the IQ-AFM mode.

Let us now briefly summarize what unique possibilities for the optical launching and probing of spin dynamics are provided by birefringence. Optical birefringence leads to modification of the incident pump-pulse polarization inside the crystal, which is responsible for the spatial distribution of the effective magnetic field induced via the inverse Faraday effect that launches magnetization oscillations. The spatial distribution of the IFE inside the crystal can be tuned by variation of the pump wavelength and polarization.

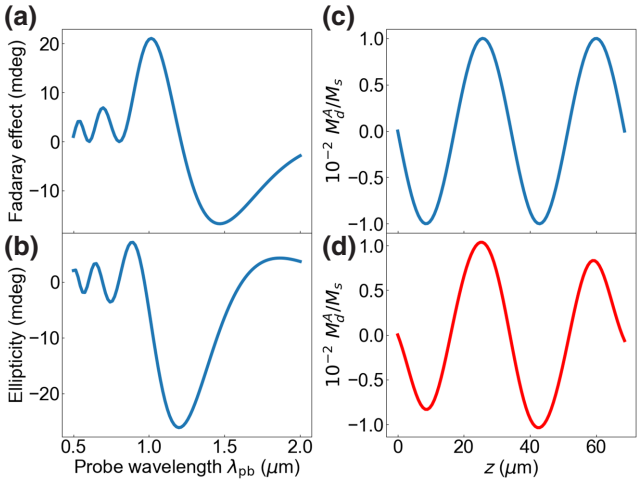

FIG. 4. The distribution of the magnetization precession amplitude induced by a pump pulse with a certain wavelength in an anisotropic material can be reconstructed (d) using the measured spectral dependences of the amplitude of the oscillations of the polarization plane (a) and ellipticity (b) of the probe pulse. (c) Real distribution of the magnetization precession amplitude in the medium.

Importantly, it is possible to investigate the temporal dynamics of such inhomogeneous modes, including modes characterized by $\int_0^L M_d^A(z)\,dz = 0$ that cannot be seen in isotropic materials, in conventional pump-probe experiments. Optical birefringence affects the magneto-optical Faraday rotation, allowing one to tune the wavelength of the probe to achieve sensitivity to any of the modes excited. Also, anisotropic crystals provide a unique possibility for reconstruction of the spatial distribution of the inhomogeneous magnetization, which can be either static (for example, in the case of a domain structure [46,48,49]) or dynamic (induced by a pump pulse as in Ref. [50], or generated via a traveling spin wave excited near the surface of the antiferromagnetic crystal [51]). Even if the spectral region where the probe measurements can be performed is limited, one can achieve good agreement with the real magnetization distribution in the medium investigated.

Acknowledgments.—This work was financially supported by the Ministry of Science and Higher Education of the Russian Federation, Megagrant Project No. 075-15-2019-1934.

[1] S. Neusser and D. Grundler, Magnonics: Spin waves on the nanoscale, Adv. Mater. **21**, 2927 (2009).
[2] L. Cornelissen, J. Liu, R. Duine, J. B. Youssef, and B. Van Wees, Long-distance transport of magnon spin information in a magnetic insulator at room temperature, Nat. Phys. **11**, 1022 (2015).
[3] K. Ganzhorn, S. Klingler, T. Wimmer, S. Geprägs, R. Gross, H. Huebl, and S. T. Goennenwein, Magnon-based logic in a multi-terminal YIG/Pt nanostructure, Appl. Phys. Lett. **109**, 022405 (2016).
[4] D. Lachance-Quirion, Y. Tabuchi, A. Gloppe, K. Usami, and Y. Nakamura, Hybrid quantum systems based on magnonics, Appl. Phys. Express **12**, 070101 (2019).
[5] D. Ignatyeva, C. Davies, D. Sylgacheva, A. Tsukamoto, H. Yoshikawa, P. Kapralov, A. Kirilyuk, V. Belotelov, and A. Kimel, Plasmonic layer-selective all-optical switching of magnetization with nanometer resolution, Nat. Commun. **10**, 1 (2019).
[6] M. R. Shcherbakov, P. P. Vabishchevich, A. S. Shorokhov, K. E. Chong, D.-Y. Choi, I. Staude, A. E. Miroshnichenko, D. N. Neshev, A. A. Fedyanin, and Y. S. Kivshar, Ultrafast all-optical switching with magnetic resonances in nonlinear dielectric nanostructures, Nano Lett. **15**, 6985 (2015).
[7] S.-J. Im, J.-S. Pae, C.-S. Ri, K.-S. Ho, and J. Herrmann, All-optical magnetization switching by counterpropagataion or two-frequency pulses using the plasmon-induced inverse Faraday effect in magnetoplasmonic structures, Phys. Rev. B **99**, 041401 (2019).
[8] D. O. Ignatyeva, D. Karki, A. A. Voronov, M. A. Kozhaev, D. M. Krichevsky, A. I. Chernov, M. Levy, and V. I. Belotelov, All-dielectric magnetic metasurface for advanced light control in dual polarizations combined with high-Q resonances, Nat. Commun. **11**, 1 (2020).
[9] Y. S. Dadoenkova, N. N. Dadoenkova, I. L. Lyubchanskii, J. W. Kłos, and M. Krawczyk, Faraday effect in bi-periodic photonic-magnonic crystals, IEEE Trans. Magn. **53**, 1 (2017).
[10] A. A. Voronov, D. Karki, D. O. Ignatyeva, M. A. Kozhaev, M. Levy, and V. I. Belotelov, Magneto-optics of sub-wavelength all-dielectric gratings, Opt. Express **28**, 17988 (2020).
[11] Y. S. Dadoenkova, F. Bentivegna, N. Dadoenkova, and I. Lyubchanskii, Transverse magneto-optic Kerr effect and Imbert–Fedorov shift upon light reflection from a magnetic/non-magnetic bilayer: Impact of misfit strain, J. Opt. **19**, 015610 (2016).
[12] O. Borovkova, D. Ignatyeva, S. Sekatskii, A. Karabchevsky, and V. Belotelov, High-Q surface electromagnetic wave resonance excitation in magnetophotonic crystals for super-sensitive detection of weak light absorption in the near-infrared, Photonics Res. **8**, 57 (2020).
[13] D. O. Ignatyeva, G. A. Knyazev, A. N. Kalish, A. I. Chernov, and V. I. Belotelov, Vector magneto-optical magnetometer based on resonant all-dielectric gratings with highly anisotropic iron garnet films, J. Phys. D: Appl. Phys. **54**, 295001 (2021).
[14] W. Tabor, A. Anderson, and L. Van Uitert, Visible and infrared Faraday rotation and birefringence of single-crystal rare-earth orthoferrites, J. Appl. Phys. **41**, 3018 (1970).
[15] F. J. Kahn, P. Pershan, and J. Remeika, Ultraviolet magneto-optical properties of single-crystal orthoferrites, garnets, and other ferric oxide compounds, Phys. Rev. **186**, 891 (1969).
[16] M. V. Chetkin and Y. I. Shcherbakov, Magneto-optical properties of orthoferrites in the infrared region of the spectrum, Solid State Phys. **11**, 1620 (1969).
[17] R. Iida, T. Satoh, T. Shimura, K. Kuroda, B. Ivanov, Y. Tokunaga, and Y. Tokura, Spectral dependence of photoinduced spin precession in $DyFeO_3$, Phys. Rev. B **84**, 064402 (2011).
[18] D. Bossini and T. Rasing, Femtosecond optomagnetism in dielectric antiferromagnets, Phys. Scr. **92**, 024002 (2017).

[19] R. Zhou, Z. Jin, G. Li, G. Ma, Z. Cheng, and X. Wang, Terahertz magnetic field induced coherent spin precession in $YFeO_3$, Appl. Phys. Lett. **100**, 061102 (2012).

[20] K. Yamaguchi, M. Nakajima, and T. Suemoto, Coherent Control of Spin Precession Motion with Impulsive Magnetic Fields of Half-Cycle Terahertz Radiation, Phys. Rev. Lett. **105**, 237201 (2010).

[21] T. H. Kim, P. Grüenberg, S. Han, and B. Cho, Field-driven dynamics and time-resolved measurement of Dzyaloshinskii-Moriya torque in canted antiferromagnet $YFeO_3$, Sci. Rep. **7**, 1 (2017).

[22] D. Bossini, S. Dal Conte, G. Cerullo, O. Gomonay, R. V. Pisarev, M. Borovsak, D. Mihailovic, J. Sinova, J. H. Mentink, T. Rasing, *et al.*, Laser-driven quantum magnonics and terahertz dynamics of the order parameter in antiferromagnets, Phys. Rev. B **100**, 024428 (2019).

[23] T. H. Kim, S. Y. Hamh, J. W. Han, C. Kang, C.-S. Kee, S. Jung, J. Park, Y. Tokunaga, Y. Tokura, and J. S. Lee, Coherently controlled spin precession in canted antiferromagnetic $YFeO_3$ using terahertz magnetic field, Appl. Phys. Express **7**, 093007 (2014).

[24] Z. Jin, Z. Mics, G. Ma, Z. Cheng, M. Bonn, and D. Turchinovich, Single-pulse terahertz coherent control of spin resonance in the canted antiferromagnet $YFeO_3$, mediated by dielectric anisotropy, Phys. Rev. B **87**, 094422 (2013).

[25] A. Reid, T. Rasing, R. Pisarev, H. Dürr, and M. Hoffmann, Terahertz-driven magnetism dynamics in the orthoferrite $DyFeO_3$, Appl. Phys. Lett. **106**, 082403 (2015).

[26] A. Kimel, A. Kirilyuk, P. Usachev, R. Pisarev, A. Balbashov, and T. Rasing, Ultrafast non-thermal control of magnetization by instantaneous photomagnetic pulses, Nature **435**, 655 (2005).

[27] A. Kimel, C. Stanciu, P. Usachev, R. Pisarev, V. Gridnev, A. Kirilyuk, and T. Rasing, Optical excitation of antiferromagnetic resonance in $TmFeO_3$, Phys. Rev. B **74**, 060403 (2006).

[28] R. Mikhaylovskiy, E. Hendry, A. Secchi, J. H. Mentink, M. Eckstein, A. Wu, R. Pisarev, V. Kruglyak, M. Katsnelson, T. Rasing, *et al.*, Ultrafast optical modification of exchange interactions in iron oxides, Nat. Commun. **6**, 1 (2015).

[29] I. Savochkin, M. Jäckl, V. Belotelov, I. Akimov, M. Kozhaev, D. Sylgacheva, A. Chernov, A. Shaposhnikov, A. Prokopov, V. Berzhansky, *et al.*, Generation of spin waves by a train of fs-laser pulses: A novel approach for tuning magnon wavelength, Sci. Rep. **7**, 1 (2017).

[30] S.-J. Im, C.-S. Ri, K.-S. Ho, and J. Herrmann, Third-order nonlinearity by the inverse Faraday effect in planar magnetoplasmonic structures, Phys. Rev. B **96**, 165437 (2017).

[31] J. De Jong, A. Kalashnikova, R. Pisarev, A. Balbashov, A. Kimel, A. Kirilyuk, and T. Rasing, Effect of laser pulse propagation on ultrafast magnetization dynamics in a birefringent medium, J. Phys.: Condens. Matter **29**, 164004 (2017).

[32] A. I. Chernov, M. A. Kozhaev, D. O. Ignatyeva, E. N. Beginin, A. V. Sadovnikov, A. A. Voronov, D. Karki, M. Levy, and V. I. Belotelov, All-dielectric nanophotonics enables tunable excitation of the exchange spin waves, Nano Lett. **20**, 5259 (2020).

[33] M. Jäckl, V. Belotelov, I. Akimov, I. Savochkin, D. Yakovlev, A. Zvezdin, and M. Bayer, Magnon Accumulation by Clocked Laser Excitation as Source of Long-Range Spin Waves in Transparent Magnetic Films, Phys. Rev. X **7**, 021009 (2017).

[34] L. Pitaevskii, Electric forces in a transparent dispersive medium, Sov. Phys. JETP **12**, 1008 (1961).

[35] J. Van der Ziel, P. S. Pershan, and L. Malmstrom, Optically-Induced Magnetization Resulting from the Inverse Faraday Effect, Phys. Rev. Lett. **15**, 190 (1965).

[36] P. Pershan, J. Van der Ziel, and L. Malmstrom, Theoretical discussion of the inverse Faraday effect, Raman scattering, and related phenomena, Phys. Rev. **143**, 574 (1966).

[37] A. Kirilyuk, A. V. Kimel, and T. Rasing, Ultrafast optical manipulation of magnetic order, Rev. Mod. Phys. **82**, 2731 (2010).

[38] D. Afanasiev, J. Hortensius, B. Ivanov, A. Sasani, E. Bousquet, Y. Blanter, R. Mikhaylovskiy, A. Kimel, and A. Caviglia, Ultrafast control of magnetic interactions via light-driven phonons, Nat. Mater. **20**, 607 (2021).

[39] P. Volkov and M. Novikov, Inverse Faraday effect in anisotropic media, Crystallogr. Rep. **47**, 824 (2002).

[40] S. Woodford, A. Bringer, and S. Blügel, Interpreting magnetization from Faraday rotation in birefringent magnetic media, J. Appl. Phys. **101**, 053912 (2007).

[41] A. Zvezdin and V. Kotov, *Modern Magnetooptics and Magnetooptical Materials* (CRC Press, Boca Raton, 1997).

[42] See Supplemental Material at http://link.aps.org/supplemental/10.1103/PhysRevApplied.16.L051001, where a detailed derivation of the expressions for the excitation, detection, and reconstruction of the magnetization dynamics is presented.

[43] A. Zvezdin, A. Kimel, D. Plokhov, and K. Zvezdin, Ultrafast spin dynamics in the iron borate easy-plane weak ferromagnet, J. Exp. Theor. Phys. **131**, 130 (2020).

[44] A. F. Andreev and V. I. Marchenko, Symmetry and the macroscopic dynamics of magnetic materials, Sov. Phys. Usp. **23**, 21 (1980).

[45] A. Zvezdin, Dynamics of domain walls in weak ferromagnets, ZhETF Pisma Redaktsiiu **29**, 605 (1979).

[46] V. G. Bar'yakhtar, B. Ivanov, and M. V. Chetkin, Dynamics of domain walls in weak ferromagnets, Sov. Phys. Usp. **28**, 563 (1985).

[47] J. De Jong, I. Razdolski, A. Kalashnikova, R. Pisarev, A. Balbashov, A. Kirilyuk, T. Rasing, and A. Kimel, Coherent Control of the Route of an Ultrafast Magnetic Phase Transition via Low-Amplitude Spin Precession, Phys. Rev. Lett. **108**, 157601 (2012).

[48] A. Pyatakov, D. Sechin, A. Sergeev, A. Nikolaev, E. Nikolaeva, A. Logginov, and A. Zvezdin, Magnetically switched electric polarity of domain walls in iron garnet films, EPL **93**, 17001 (2011).

[49] A. S. Logginov, G. Meshkov, A. V. Nikolaev, and A. P. Pyatakov, Magnetoelectric control of domain walls in a ferrite garnet film, JETP Lett. **86**, 115 (2007).

[50] D. Afanasiev, B. Ivanov, A. Kirilyuk, T. Rasing, R. Pisarev, and A. Kimel, Control of the Ultrafast Photoinduced Magnetization Across the Morin Transition in $DyFeO_3$, Phys. Rev. Lett. **116**, 097401 (2016).

[51] J. Hortensius, D. Afanasiev, M. Matthiesen, R. Leenders, R. Citro, A. Kimel, R. Mikhaylovskiy, B. Ivanov, and A. Caviglia, Coherent spin-wave transport in an antiferromagnet, Nat. Phys. **17**, 1001 (2021).